ANALYTICAL APPROACH TO CHANNELIZED HOTELLING OBSERVER PERFORMANCE FOR REGULARIZED TOMOGRAPHIC IMAGE RECONSTRUCTION

Anastasia Yendiki and Jeffrey A. Fessler

The University of Michigan
Dept. of Electrical Engineering and Computer Science
1301 Beal Ave.
Ann Arbor, MI 48109-2122, USA

ABSTRACT

Our goal is to analyze regularized image reconstruction methods such as penalized likelihood with respect to the performance of the Channelized Hotelling Observer (CHO) in the task of detecting a small target signal in the reconstructed images, in the presence of a correlated random background. We derive here an approximation to the performance of the CHO by working entirely with continuous-space formulations and then discretizing the final result. This approach leads to an extension and a refinement of approximations that we previously derived in the discrete space.

1. INTRODUCTION

Several types of medical diagnosis involve the detection of a small abnormality in an image reconstructed from noisy tomographic data. Image reconstruction methods abound and several of them involve user-specified parameters (such as the regularization parameter in penalized-likelihood reconstruction or the filter cut-off in filtered back-projection). Such parameters control the noise/resolution trade-off and can have a dramatic effect on the appearance of the reconstructed images. To avoid the subjectivity of judging by appearances, it is useful to examine how the choice of reconstruction method and/or parameter affects some objective figure of merit, such as the performance of an observer faced with the task of detecting a lesion in the reconstructed image. As the performance of human observers does not lend itself to optimization through analytical tools, we turn to the various mathematical observers that exist in the literature [1, §14.3]. In particular, we focus on the Channelized Hotelling Observer (CHO) [2], whose performance has been found to be correlated with that of human observers for some simple detection tasks (*e.g.*, see [3]). In [4] we analyzed the performance of this observer paired with regularized image reconstruction in the detection of a statistically varying signal at a known location on a deterministic background. Our analysis showed that regularization is not essential for this simple detection task. However, the performance of human and model observers alike is known to deteriorate in the presence of a correlated image background, as the detection task becomes more complex [5]. In this paper, we extend our analysis to accommodate statistically-varying backgrounds. Furthermore, our approach here is distinct from the one we followed in [4] and instead parallels the one followed in [6] for roughness penalty design; we now perform the analysis entirely in the continuous domain and discretize the final result. This approach leads to a refinement of our approximations. Our new findings reduce to the ones we derived in the discrete domain in [4] only under certain assumptions on the statistics of the problem.

Work supported in part by NSF grant BES-9982349.

2. CONTINUOUS-SPACE SYSTEM MODEL

Let $\boldsymbol{f} \in \mathcal{L}_2(\mathbb{R}^2)$ be the object of interest. The detection task at hand is to determine between the following pair of hypotheses:

$$\begin{aligned} H_0 &: \quad \boldsymbol{f} = \boldsymbol{b} \\ H_1 &: \quad \boldsymbol{f} = \boldsymbol{b} + \boldsymbol{x}, \end{aligned} \tag{1}$$

where $\boldsymbol{b} \in \mathcal{L}_2(\mathbb{R}^2)$ is the random object background and covariance $\mathcal{K}_{\boldsymbol{b}}$, and $\boldsymbol{x} \in \mathcal{L}_2(\mathbb{R}^2)$ is a spatially-localized target signal, which is deterministic and known. The decision is based on the observed data $\boldsymbol{y} \in \mathcal{L}_2([0,\pi] \times \mathbb{R})$, given by

$$\boldsymbol{y} = \mathcal{A}\boldsymbol{f} + \boldsymbol{\varepsilon}, \tag{2}$$

where $\mathcal{A} : \mathcal{L}_2(\mathbb{R}^2) \rightarrow \mathcal{L}_2([0,\pi] \times \mathbb{R})$ is a linear operator modeling the imaging system, and $\boldsymbol{\varepsilon} \in \mathcal{L}_2([0,\pi] \times \mathbb{R})$ is zero-mean noise with covariance $\mathcal{K}_{\boldsymbol{\varepsilon}}$.

In its most general form, the linear operator $\mathcal{A}$ will be described by a superposition integral, possibly accounting for position-dependent characteristics of the imaging system:

$$\boldsymbol{p} = \mathcal{A}\boldsymbol{f} \Leftrightarrow p_\varphi(r) = \int_{-\infty}^{\infty} \int_{-\infty}^{\infty} a(r,\varphi;x,y) f(x,y) \, \mathrm{d}x \, \mathrm{d}y.$$

However, the analysis can be greatly simplified by assuming the following separable form:

$$\boldsymbol{\mathcal{A}} = \boldsymbol{\mathcal{B}}\boldsymbol{\mathcal{P}}, \tag{3}$$

where $\boldsymbol{\mathcal{P}} : \mathcal{L}_2(\mathbb{R}^2) \rightarrow \mathcal{L}_2([0,\pi] \times \mathbb{R})$ is the Radon transform operator and $\boldsymbol{\mathcal{B}} : \mathcal{L}_2([0,\pi] \times \mathbb{R}) \rightarrow \mathcal{L}_2([0,\pi] \times \mathbb{R})$ is the system blur operator.

If the system blur is shift-invariant with respect to radial position r, and its impulse response at projection angle φ is $b_\varphi(r)$, then $\boldsymbol{\mathcal{B}} = (\boldsymbol{\mathcal{I}} \otimes \boldsymbol{\mathcal{U}}_1)^{-1}\boldsymbol{\mathcal{D}}(B_\varphi(\rho))(\boldsymbol{\mathcal{I}} \otimes \boldsymbol{\mathcal{U}}_1)$, where $\otimes$ signifies the Kronecker product, $\boldsymbol{\mathcal{I}}$ is the identity operator, $\boldsymbol{\mathcal{U}}_n$ is the n-D continuous-space Fourier transform, $\boldsymbol{\mathcal{D}}(\cdot)$ performs point-by-point multiplication (thus it is a continuous space "diagonal" operator) and $B_\varphi(\rho)$ is the 1-D Fourier transform of $b_\varphi(r)$. In that case, the separable form of $\boldsymbol{\mathcal{A}}$ in (3) is exact. Eventually we will be applying the operator to objects that are highly localized around some pixel j, so we can also accommodate systems that are shift-variant, as long as they can be considered locally shift-invariant around pixel j. In that case, the separable form in (3) can be used as an approximation with

$$\boldsymbol{\mathcal{B}} = (\boldsymbol{\mathcal{I}} \otimes \boldsymbol{\mathcal{U}}_1)^{-1}\boldsymbol{\mathcal{D}}(B_\varphi^j(\rho))(\boldsymbol{\mathcal{I}} \otimes \boldsymbol{\mathcal{U}}_1), \tag{4}$$

where $B_\varphi^j(\rho)$ is the 1-D Fourier transform of $b_\varphi^j(r)$, which is the blur that pixel j experiences when projected at angle φ.

We can apply the Singular Value Decomposition (SVD) of the 2-D Radon transform operator, as presented in [1, p. 1174], to write $\boldsymbol{\mathcal{P}} = \boldsymbol{\mathcal{V}}\boldsymbol{\mathcal{D}}(|\rho|^{-1/2})\boldsymbol{\mathcal{U}}_2$, where $\boldsymbol{\mathcal{V}} = \boldsymbol{\mathcal{I}} \otimes (\boldsymbol{\mathcal{U}}_1^{-1}\boldsymbol{\mathcal{D}}(|\rho|^{1/2}))$. One can show that $\boldsymbol{\mathcal{V}}$ is a unitary operator. This SVD form can be used to easily confirm that

$$\begin{aligned} \boldsymbol{\mathcal{P}}^*\boldsymbol{\mathcal{P}} &= \boldsymbol{\mathcal{U}}_2^{-1}\boldsymbol{\mathcal{D}}(|\rho|^{-1})\boldsymbol{\mathcal{U}}_2 \\ \boldsymbol{\mathcal{P}}\boldsymbol{\mathcal{P}}^* &= \boldsymbol{\mathcal{V}}\boldsymbol{\mathcal{D}}(|\rho|^{-1})\boldsymbol{\mathcal{V}}^* = \boldsymbol{\mathcal{I}} \otimes (\boldsymbol{\mathcal{U}}_1^{-1}\boldsymbol{\mathcal{D}}(|\rho|^{-1})\boldsymbol{\mathcal{U}}_1). \end{aligned}$$

3. CHO PERFORMANCE

In clinical practice a human observer would typically attempt to detect a lesion by examining an image reconstructed from the raw data, rather than examining the raw data itself. Therefore we focus on mathematical observers that are applied to reconstructed images.

To facilitate analysis, we consider here linear reconstructors. Common tomographic reconstruction techniques can be approximated as linear, except maybe when enforcing a non-negativity constraint. Here we will assume that the target signal appears on a background that is sufficiently high to render the non-negativity constraint inactive. Thus we proceed to define a linear reconstruction operator $\boldsymbol{\mathcal{S}} : \mathcal{L}_2([0,\pi] \times \mathbb{R}) \rightarrow \mathcal{L}_2(\mathbb{R}^2)$. The reconstructed image is then given by $\hat{\boldsymbol{f}}(\boldsymbol{y}) = \boldsymbol{\mathcal{S}}\boldsymbol{y}$.

Channelized observer models attempt to mimic the human visual system by filtering their input through a set of M frequency-selective channels and keeping only the output of each filter at the spatial position j of the target signal. Let $\boldsymbol{\mathcal{C}} : \mathbb{C}^M \rightarrow \mathcal{L}_2(\mathbb{R}^2)$ be the operator describing this filtering, so that the output of the channels is given by $\hat{\boldsymbol{c}}(\boldsymbol{y}) = \boldsymbol{\mathcal{C}}^*\hat{\boldsymbol{f}}(\boldsymbol{y}) = \boldsymbol{\mathcal{C}}^*\boldsymbol{\mathcal{S}}\boldsymbol{y}$. One can view $\boldsymbol{\mathcal{C}}$ as a collection of operators arranged in a $1 \times M$ row vector. The m-th element of this vector is an operator $\boldsymbol{\mathcal{C}}_m : \mathbb{C} \rightarrow \mathcal{L}_2(\mathbb{R}^2)$ such that

$$\boldsymbol{\mathcal{C}}_m^* = \boldsymbol{\Delta}_j\boldsymbol{\mathcal{U}}_2^{-1}\boldsymbol{\mathcal{D}}(C_m^*(\rho,\Phi))\boldsymbol{\mathcal{U}}_2,$$

where $C_m(\rho,\Phi)$ is the frequency response of the m-th channel and $\boldsymbol{\Delta}_j : \mathcal{L}_2(\mathbb{R}^2) \rightarrow \mathbb{R}$ is an operator sampling a single point from a continuous-space function. This operator and its adjoint can be defined in terms of the Dirac $\boldsymbol{\delta}$ function:

$$\begin{aligned} \alpha = \boldsymbol{\Delta}_j\boldsymbol{f} \quad &\Leftrightarrow \quad \alpha = \boldsymbol{f}(x - x_j, y - y_j) \\ \boldsymbol{f} = \boldsymbol{\Delta}_j^*\alpha \quad &\Leftrightarrow \quad \boldsymbol{f}(x,y) = \alpha\boldsymbol{\delta}(x - x_j, y - y_j). \end{aligned}$$

A general linear channelized observer applies a template $\boldsymbol{w} \in \mathbb{R}^M$ to the channel output and evaluates a test statistic of the form

$$t(\boldsymbol{y}) = \langle \boldsymbol{w},\, \hat{\boldsymbol{c}}(\boldsymbol{y}) \rangle = \langle \boldsymbol{w},\, \boldsymbol{\mathcal{C}}^*\boldsymbol{\mathcal{S}}\boldsymbol{y} \rangle. \tag{5}$$

The observer then decides that H_1 is true (*i.e.*, the signal is present) only if this test statistic exceeds a certain threshold. In particular, the template applied by the CHO is

$$\boldsymbol{w}_{\text{CHO}} = (\,\text{Cov}\{\hat{\boldsymbol{c}}\})^\dagger(E[\hat{\boldsymbol{c}}|H_1] - E[\hat{\boldsymbol{c}}|H_0]). \tag{6}$$

A useful detection performance metric is the area under the Receiver Operating Characteristic (ROC) curve. The area under the ROC curve is difficult to compute in general, but in the case of Gaussian-distributed test statistics it is directly related to the Signal-to Noise Ratio (SNR), which is considerably easier to compute:

$$\text{SNR}^2 = \frac{\left(E[t|H_1] - E[t|H_0]\right)^2}{\text{Var}\{t\}}. \tag{7}$$

Even if the observed data is not Gaussian, the test statistic may be assumed to be Gaussian by invoking the central limit theorem. Therefore we consider the SNR as a performance metric hereafter.

Combining (1), (2), and (5) – (7) leads to

$$\text{SNR}_{\text{CHO}}^2 \quad = \quad \langle \boldsymbol{W}^\dagger\boldsymbol{z},\, \boldsymbol{z} \rangle, \tag{8}$$

where we define $\boldsymbol{W} \in \mathbb{C}^{M \times M}$ and $\boldsymbol{z} \in \mathbb{C}^M$ such that

$$\begin{aligned} \boldsymbol{W} &\triangleq \boldsymbol{\mathcal{C}}^*\boldsymbol{\mathcal{S}}\boldsymbol{\mathcal{K}}\boldsymbol{\mathcal{S}}^*\boldsymbol{\mathcal{C}} \\ \boldsymbol{z} &\triangleq \boldsymbol{\mathcal{C}}^*\boldsymbol{\mathcal{S}}\boldsymbol{\mathcal{A}}\boldsymbol{x} \end{aligned} \tag{9}$$

and where $\boldsymbol{\mathcal{K}} = \boldsymbol{\mathcal{K}}_{\boldsymbol{\varepsilon}} + \boldsymbol{\mathcal{A}}\,\boldsymbol{\mathcal{K}}_{\boldsymbol{b}}\,\boldsymbol{\mathcal{A}}^*$ is the covariance of the data $\boldsymbol{y}$. The covariance operator $\boldsymbol{\mathcal{K}}_{\boldsymbol{b}}$ is defined by a superposition integral as follows:

$$\boldsymbol{g} = \boldsymbol{\mathcal{K}}_{\boldsymbol{b}}\boldsymbol{f} \Leftrightarrow \boldsymbol{g}(\vec{r}) = \int_\infty \text{Cov}\{b(\vec{r}), b(\vec{r}')\}\,\boldsymbol{f}(\vec{r}')d\vec{r}'$$

and the other covariance operators are defined similarly.

4. CHO WITH PWLS RECONSTRUCTION

We would like to investigate the performance of the CHO when the observer is applied to images produced by regularized reconstruction methods. For simplicity we focus here on unconstrained PWLS reconstruction. However, such analysis can be extended to penalized likelihood [7]. Unconstrained PWLS with the usual $\boldsymbol{\mathcal{K}}^{-1}$ weighting reduces to

$$\begin{aligned}\hat{\boldsymbol{f}}(\boldsymbol{y}) &= \arg\min_{\boldsymbol{f}} \Big\{ \frac{1}{2}||\boldsymbol{y}-\boldsymbol{\mathcal{A}}\boldsymbol{f}||^2_{\boldsymbol{\mathcal{K}}^{-1/2}} + \frac{1}{2}\beta\langle \boldsymbol{f},\, \boldsymbol{\mathcal{R}}\boldsymbol{f}\rangle \Big\} \\ &= (\boldsymbol{\mathcal{F}}+\boldsymbol{\mathcal{R}})^{-1}\boldsymbol{\mathcal{A}}^*\boldsymbol{\mathcal{K}}^{-1}\boldsymbol{y} = \boldsymbol{\mathcal{S}}\boldsymbol{y} \qquad (10)\end{aligned}$$

where $\boldsymbol{\mathcal{F}} : \mathcal{L}_2(\mathbb{R}^2) \to \mathcal{L}_2(\mathbb{R}^2)$ is a Fisher information operator defined by $\boldsymbol{\mathcal{F}} \triangleq \boldsymbol{\mathcal{A}}^*\boldsymbol{\mathcal{K}}^{-1}\boldsymbol{\mathcal{A}}$ and $\boldsymbol{\mathcal{R}} : \mathcal{L}_2(\mathbb{R}^2) \to \mathcal{L}_2(\mathbb{R}^2)$ is a roughness penalty operator.

By substituting the PWLS reconstructor (10) into the expressions (9) we end up with

$$\begin{aligned}\boldsymbol{W} &= \boldsymbol{\mathcal{C}}^*(\boldsymbol{\mathcal{F}}+\boldsymbol{\mathcal{R}})^{-1}\boldsymbol{\mathcal{F}}(\boldsymbol{\mathcal{F}}+\boldsymbol{\mathcal{R}})^{-1}\boldsymbol{\mathcal{C}} \\ \boldsymbol{z} &= \boldsymbol{\mathcal{C}}^*(\boldsymbol{\mathcal{F}}+\boldsymbol{\mathcal{R}})^{-1}\boldsymbol{\mathcal{F}}\boldsymbol{x}. \qquad (11)\end{aligned}$$

These exact expressions involve rather intensive computation. However, by assuming that the target signal $\boldsymbol{x}$ is highly localized around some pixel j and that the operators in (11) can be assumed locally shift-invariant around j, we can develop a Fourier-space approximation of the SNR.

The Fisher information operator $\boldsymbol{\mathcal{F}}_{\boldsymbol{\varepsilon}}$ for the case of no object variability ($\boldsymbol{\mathcal{F}}_{\boldsymbol{\varepsilon}} \triangleq \boldsymbol{\mathcal{A}}^*\boldsymbol{\mathcal{K}}_{\boldsymbol{\varepsilon}}^{-1}\boldsymbol{\mathcal{A}}$) is analyzed in [6] using the local shift invariance assumption in (4). The resulting approximation is

$$\begin{aligned}\boldsymbol{\mathcal{F}}_{\boldsymbol{\varepsilon}} &\approx \boldsymbol{\mathcal{U}}_2^{-1}\boldsymbol{\mathcal{D}}\Big(\frac{w_j(\Phi)\,|B^j_\Phi(\rho)\,|^2}{|\rho|}\Big)\boldsymbol{\mathcal{U}}_2 \\ &\triangleq \boldsymbol{\mathcal{U}}_2^{-1}\boldsymbol{\mathcal{D}}(F_{\boldsymbol{\varepsilon}}(\rho,\Phi))\boldsymbol{\mathcal{U}}_2,\end{aligned}$$

where we define

$$w_j(\varphi) \triangleq \frac{\int_{-\infty}^{\infty} |a(r,\varphi;x_j,y_j)|^2\, \frac{1}{\sigma^2_{\boldsymbol{\varepsilon}}(r,\varphi)}\,\mathrm{d}r}{\int_{-\infty}^{\infty} |a(r,\varphi;x_j,y_j)|^2\,\mathrm{d}r}$$

to be the local angle-dependent uncertainties corresponding to the spatial position (x_j, y_j). This is the position of the pixel j around which we know our target signal to be concentrated. The $\sigma^2_{\boldsymbol{\varepsilon}}(r,\varphi)$ factors are the variances of the independent noise random variables $\boldsymbol{\varepsilon}(r,\varphi)$. For a practical implementation, one would need to discretize the integrals above. Even so, these discretized local uncertainties would provide a more refined approximation that the angle-independent local uncertainties derived directly in the discrete domain and used in [4].

We now generalize the previous result to include background variability. One can show that:

$$\begin{aligned}\boldsymbol{\mathcal{F}} &\approx \boldsymbol{\mathcal{U}}_2^{-1}\boldsymbol{\mathcal{D}}\Big(\frac{F_{\boldsymbol{\varepsilon}}(\rho,\Phi)}{1+F_{\boldsymbol{\varepsilon}}(\rho,\Phi)K_b(\rho,\Phi)}\Big)\boldsymbol{\mathcal{U}}_2 \\ &\triangleq \boldsymbol{\mathcal{U}}_2^{-1}\boldsymbol{\mathcal{D}}(F(\rho,\Phi))\boldsymbol{\mathcal{U}}_2,\end{aligned}$$

where $K_b(\rho,\Phi)$ is the power spectrum of $\boldsymbol{b}$ (assuming that $\boldsymbol{\mathcal{K}}_{\boldsymbol{b}}$ is locally shift-invariant). For $K_b(\cdot,\cdot) = 0$, the expression above reduces to the one in [6].

Assuming that $X(\rho,\Phi)$ is the spectrum of the target signal $\boldsymbol{x}$ and $R(\rho,\Phi)$ the frequency response of the regularizer $\boldsymbol{\mathcal{R}}$ (locally around the position j of the target signal), then we can approximate (11) as

$$\begin{aligned}\boldsymbol{W} &\approx \boldsymbol{\mathcal{C}}^*\boldsymbol{\mathcal{U}}_2^{-1}\boldsymbol{\mathcal{D}}\Big(\frac{F(\rho,\Phi)}{[F(\rho,\Phi)+R(\rho,\Phi)]^2}\Big)\boldsymbol{\mathcal{U}}_2\boldsymbol{\mathcal{C}} \\ \boldsymbol{z} &\approx \boldsymbol{\mathcal{C}}^*\boldsymbol{\mathcal{U}}_2^{-1}\Big(\frac{X(\rho,\Phi)F(\rho,\Phi)}{F(\rho,\Phi)+R(\rho,\Phi)}\Big). \qquad (12)\end{aligned}$$

Also, consider any locally shift-invariant system $\boldsymbol{\mathcal{H}}$ with local impulse response and frequency response $h_j(x,y)$ and $H_j(\rho,\Phi)$ respectively. One can show that applying the operator $\boldsymbol{\Delta}_j\boldsymbol{\mathcal{H}}$ on an object highly localized around j is approximately equivalent to scaling the object by a factor of $h_j(0,0) = \iint H_j(\rho,\Phi)\rho d\rho d\Phi$. By applying this property to the definition of $\boldsymbol{\mathcal{C}}$, we can approximate the (m,n) element of $\boldsymbol{W}$ as

$$[\boldsymbol{W}]_{mn} \approx \iint \frac{C_m(\rho,\Phi)C_n^*(\rho,\Phi)F(\rho,\Phi)}{[F(\rho,\Phi)+R(\rho,\Phi)]^2}\rho d\rho d\Phi \qquad (13)$$

and the m-th element of $\boldsymbol{z}$ as

$$[\boldsymbol{z}]_m \approx \iint \frac{C_m(\rho,\Phi)X(\rho,\Phi)F(\rho,\Phi)}{F(\rho,\Phi)+R(\rho,\Phi)}\rho d\rho d\Phi. \qquad (14)$$

In general we won't be able to perform the inversion in (8) analytically. However, in the special case of CHO channels with non-overlapping passbands, $\boldsymbol{W}$ becomes diagonal and by substituting (13) and (14) into (8) we get

$$\mathrm{SNR}^2_{\text{CHO,PWLS}} \approx \sum_{m=1}^{M} \frac{|\iint C_m(\rho,\Phi)\frac{X(\rho,\Phi)F(\rho,\Phi)}{F(\rho,\Phi)+R(\rho,\Phi)}\rho d\rho d\Phi|^2}{\iint |C_m(\rho,\Phi)|^2\frac{F(\rho,\Phi)}{[F(\rho,\Phi)+R(\rho,\Phi)]^2}\rho d\rho d\Phi}.$$

We now discretize this result and produce the following SNR approximation for CHO/PWLS with non-overlapping passbands:

$$\mathrm{SNR}^2_{\text{CHO,PWLS}} \approx \sum_{m=1}^{M} \frac{\Big|\sum_k C_k X_k \frac{F_k}{F_k+R_k}\Big|^2}{\sum_k |C_k|^2 \frac{F_k}{(F_k+R_k)^2}}, \qquad (15)$$

where all variables are in discrete space, k indexes DFT vectors, $\{C_k\}$ is the frequency response of the m-th channel, $\{X_k\}$ is the spectrum of the target signal, $\{R_k\}$ the spectrum of the regularizer, and $\{F_k\}$ is the frequency response of the Fisher information matrix. All DFT's above are taken locally at pixel j. It turns out that the approximation we proposed in [4] can be derived as a special case of (15) with certain assumptions about the object statistics.

5. RESULTS

As an example of using the approximate SNR expression in (15) to choose the regularization parameter β for PWLS reconstruction, we consider the case of a 2-D SPECT system model with depth-dependent system blur, an image size of 64×64 pixels, and an impulse as the target signal. We assume that the background $\boldsymbol{b}$ has a Gaussian autocorrelation function (ACF). For the measurement noise $\boldsymbol{\varepsilon}$, we use covariances equal to $\sigma_{\boldsymbol{\varepsilon}}^2(k) = [\boldsymbol{A}\boldsymbol{x}_0]_k$, where $\boldsymbol{A}$ is the system matrix and $\boldsymbol{x}_0$ an anthropomorphic phantom.

We evaluate the SNR of the CHO using the approximation in (15) for PWLS with first-order quadratic regularization and various values of the regularization parameter β, as well as various degrees of background correlation. Figure 1 shows the SNR (normalized with respect to the SNR of the ideal observer) vs. the regularization parameter β for two distinct cases: no background variability and a highly correlated background whose ACF is a Gaussian with a FWHM of $\sim$12 pixels. Plots are shown for two different CHO's; one has 6 channels with non-overlapping radially-symmetric dyadic passbands, and one has a single all-pass channel.

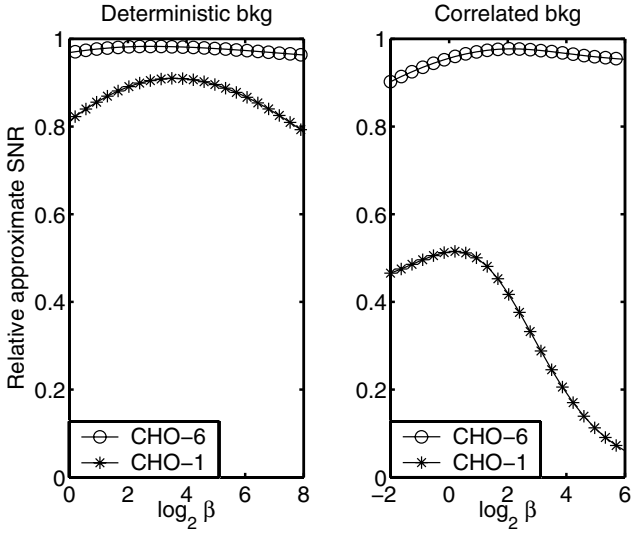

Fig. 1. Approximate SNR of the CHO vs. regularization parameter β, assuming no background variability (left plot) and a Gaussian background ACF with a FWHM of $\sim$12 pixels (right plot). Plots are shown for two different CHO's; one has 6 channels with non-overlapping radially-symmetric dyadic passbands (CHO-6), and one has a single all-pass channel (CHO-1).

6. DISCUSSION

Our preliminary results show a degradation of CHO performance in the presence of correlated random noise. The degradation is of course not as dramatic in the (more realistic) case of the CHO with 6 channels when compared to the CHO with a single all-pass channel, as the latter imposes a rather drastic loss of information on the data. However, even in the case of the CHO with 6 channels, the SNR plot departs from the flatness that characterized it without background variability.

Our approximations can be used for a fast computation of CHO performance in a wide variety of cases. We intend to further investigate these approximations and their accuracy. In particular, it is of interest to examine the effect of more realistic channels (with non-flat and potentially overlapping passbands), internal observer noise, and signal location variability.

7. REFERENCES

[1] H. H. Barrett and K. J. Meyers, *Foundations of image science*, Wiley, New York, 2003.

[2] K. J. Myers and H. H. Barrett, "Addition of a channel mechanism to the ideal-observer model," *J. Opt. Soc. Am. A*, vol. 4, no. 12, pp. 2447–57, Dec. 1987.

[3] C. K. Abbey and H. H. Barrett, "Human- and model-observer performance in ramp-spectrum noise: effects of regularization and object variability," *J. Opt. Soc. Am. A*, vol. 18, no. 3, pp. 473–88, Mar. 2001.

[4] J. A. Fessler and A. Yendiki, "Channelized Hotelling observer performance for penalized-likelihood image reconstruction," in *Proc. IEEE Nuc. Sci. Symp. Med. Im. Conf.*, 2002, vol. 2, pp. 1040–4.

[5] J. P. Rolland and H. H. Barrett, "Effect of random background inhomogeneity on observer detection performance," *J. Opt. Soc. Am. A*, vol. 9, no. 5, pp. 649–58, May 1992.

[6] J. A. Fessler, "Analytical approach to regularization design for isotropic spatial resolution," in *Proc. IEEE Nuc. Sci. Symp. Med. Im. Conf.*, 2003, To appear. 1343, M5-5.

[7] J. A. Fessler, "Mean and variance of implicitly defined biased estimators (such as penalized maximum likelihood): Applications to tomography," *IEEE Tr. Im. Proc.*, vol. 5, no. 3, pp. 493–506, Mar. 1996.